Please cite the Published Version

Fritz, Hans, Ray, Nicola, Dyrba, Martin, Sorg, Christian, Teipel, Stefan and Grothe, Michel (2019) The corticotopic organization of the human basal forebrain as revealed by regionally selective functional connectivity profiles. Human Brain Mapping, 40 (3). pp. 868-878. ISSN 1065-9471

DOI: https://doi.org/10.1002/hbm.24417

Publisher: Wiley

Version: Accepted Version

HUMAN BRAIN MAPPING

The corticotopic organization of the human basal forebrain as revealed by regionally selective functional connectivity profiles

Journal:	Human Brain Mapping
Manuscript ID	HBM-18-0390.R1
Wiley - Manuscript type:	Research Article
Date Submitted by the Author:	06-Aug-2018
Complete List of Authors:	Fritz, Hans-Christian J.; Deutsches Zentrum fur Neurodegenerative Erkrankungen, Ray, Nicola; Manchester Metropolitan University Department of Psychology Dyrba, Martin; DZNE, Site Rostock/Greifswald, ; MMIS Group, University of Rostock, Department of Computer Science Sorg, Christian; Technische Universität München, Department of Psychiatry and Psychotherapy, Department of Neuroradiology Teipel, Stefan; DZNE, Grothe, Michel; German Center for Neurodegenerative Diseases (DZNE), Site Rostock/ Greifswald
Keywords:	resting-state functional MRI, basal forebrain, functional connectivity, functional clustering, connectivity-based parcellation

The corticotopic organization of the human basal forebrain as revealed by regionally selective functional connectivity profiles

Abbreviatedtitle: Cortical connectivity of the basal forebrain

Hans-Christian J. Fritz [1,2], Nicola Ray [3], Martin Dyrba [1], Christian Sorg [4], Stefan Teipel [1,2], Michel J. Grothe [1*]

[1] German Center for Neurodegenerative Diseases (DZNE), Site Rostock/Greifswald, 18147 Rostock, Germany

[2] Clinic of Psychosomatic and Psychotherapeutic Medicine, Rostock University Medical Center, 18147 Rostock, Germany

[3] Department of Psychology, Manchester Metropolitan University, Manchester, UK

[4] TUM-Neuroimaging Center of Klinikum rechts der Isar, Departments of Neuroradiology and Psychiatry, Technische Universität München TUM, 81675 Munich, Germany

*Corresponding author:

Michel J. Grothe

German Center for Neurodegenerative Diseases (DZNE)

Gehlsheimer Str. 20, D-18147 Rostock, Germany

E-mail: Michel.Grothe@dzne.de

Phone: +49 (0) 381 / 494 - 9479

Word counts: Abstract, 250 words; Manuscript text, 4252 words

References: 82

Tables: 2

Figures: 5

Acknowledgements

We would like to thank the International Data-Sharing Initiative (INDI; http://fcon_1000.projects.nitrc.org/indi/) and all contributing institutions for openly sharing their valuable neuroimaging data sets. Parts of the presented material arise from the doctoral thesis of H.-C. F.

Conflict of interest: The authors declare no competing financial interests or relationships.

Abstract

The cholinergic basal forebrain (CBF), comprising different groups of cortically projecting cholinergic neurons, plays a crucial role in higher cognitive processes and has been implicated in diverse neuropsychiatric disorders. A distinct corticotopic organization of CBF projections has been revealed in animal studies, but little is known about their organization in the human brain. We explored regional differences in functional connectivity (FC) profiles within the human CBF by applying a clustering approach to resting-state functional MRI (rs-fMRI) data of healthy adult individuals of both sexes (N=85; 19-85y). We further examined effects of age on FC of the identified CBF clusters, and assessed the reproducibility of cluster-specific FC profiles in independent data from healthy older individuals (N=25; 65-89y). Results showed that the human CBF is functionally organized into distinct anterior-medial and posterior-lateral subdivisions that largely follow anatomically defined boundaries of the medial septum/diagonal band and nucleus basalis Meynert (NBM), respectively, with a transitional zone in the anterior-medial NBM. The anterior-medial CBF subdivision was characterized by connectivity with the hippocampus and interconnected nodes of an extended medial cortical memory network, whereas the posterior-lateral subdivision was specifically connected to anterior insula and dorsal anterior cingulate components of a salience/attention network. FC of both CBF subdivisions declined with increasing age, but the overall topography of subregion-specific FC profiles was reproduced in independent rs-fMRI data of healthy older individuals acquired in a typical clinical setting. Rs-fMRI-based assessments of subregion-specific CBF function may complement established volumetric approaches for the in-vivo study of CBF involvement in neuropsychiatric disorders.

Keywords: resting-state functional MRI, basal forebrain, functional connectivity, functional clustering, connectivity-based parcellation

Introduction

Nuclei of cholinergic neurons in the basal forebrain innervate the entire cerebral cortex and limbic structures such as the hippocampus (Luiten, et al., 1987; Mesulam, et al., 1983a). Corticopetal signaling from the cholinergic basal forebrain (CBF) modulates neuronal activity in its cortical target regions and has been implicated in attentional processes as well as in synaptic plasticity, learning and memory (Ballinger, et al., 2016; Hasselmo and Sarter, 2011). Dysfunction of the CBF has been associated with a range of neuropsychiatric disorders, including schizophrenia (Sarter, et al., 2012), autism (Perry, et al., 2001), Alzheimer's disease and Lewy body disease (Rogers, et al., 1985; Whitehouse, et al., 1983; Whitehouse, et al., 1982).

According to Mesulam's nomenclature (Mesulam, et al., 1983a; Mesulam, et al., 1983b), the CBF can be cytoarchitectonically subdivided from anterior to posterior into four main cell groups (Ch1-4), which reflect cholinergic neurons of the medial septum (MS, Ch1), the vertical (Ch2) and horizontal (Ch3) limb of the diagonal band of Broca (DB), and the nucleus basalis Meynert (NBM, Ch4). The NBM represents the largest cluster of cholinergic neurons within the CBF and can be further subdivided into anterior-medial and -lateral (Ch4am, Ch4al), intermediate (Ch4i) and posterior (Ch4p) sections based on anatomo-topographic characteristics. Evidence from axonal tracer studies in rodents and nonhuman primates indicates that CBF neurons project to the cortex in a distinct topographic organization. Thus, anterior-medial cell clusters of the CBF project predominantly to the hippocampus and ventromedial cortical regions, whereas the projection density progressively shifts to lateral neocortical areas for more posterior-lateral cell clusters (Bloem, et al., 2014; Ghashghaei and Barbas, 2001; Luiten, et al., 1987; Mesulam, et al., 1983a; Zaborszky, et al., 2015). In the human brain, cholinergic cell clusters are arranged in a similar anatomic topography within the CBF (Hedreen, et al., 1984; Mesulam and Geula, 1988), and the cholinergic pathways

(Kitt, et al., 1987; Mesulam, et al., 1992; Selden, et al., 1998). However, given that direct axonal tracing studies are not feasible in humans, little is known about the corticotopic organization of CBF projections in the human brain (Mesulam and Geula, 1988).

Over the last years, functional connectivity (FC) analysis of resting-state functional MRI (rs-fMRI) data has emerged as a powerful in-vivo tool to study interconnected neuronal systems and subcortical-cortical interactions in the human brain (Englot, et al., 2017; Libby, et al., 2012; Roy, et al., 2009; Zhang, et al., 2016). This method has previously been used to characterize the FC profile of the NBM using a seed region derived from a cytoarchitectonically-defined stereotactic atlas of CBF nuclei (Li, et al., 2014; Zaborszky, et al., 2008). While this study provided unprecedented insight into the cortical connectivity of the NBM in the human brain, it was limited in scope by the focus on an a priori defined NBM seed region. More recently, connectivity differences between CBF subdivisions were explored using rs-fMRI data from young adults (Markello, et al., 2018), but not yet across a wider age range or in an older population.

In the present study we used FC-based parcellation of the CBF as a well-established data-driven approach for studying FC characteristics of presumably functionally heterogeneous brain regions (Eickhoff, et al., 2015; Kahnt, et al., 2012; Mishra, et al., 2014; Pascual, et al., 2015; Zhang, et al., 2010; Zhuo, et al., 2016). Parcellation was based on a comprehensive cytoarchitectonically-defined spatial outline of the CBF without predefined segments. Based on the distinct corticotopic organization of CBF projections observed in rodents and nonhuman primates, we hypothesized that the human CBF may be parcellated into at least two clearly functionally-distinct subdivisions along its anterior-posterior axis that reflect the previously described preferential projections to hippocampus/ventromedial cortex and lateral neocortical areas, respectively. We then characterized the identified CBF FC profiles in relation to well described cortical functional networks (Yeo, et al., 2011), reproducibility of subdivision-specific FC patterns in independent rs-fMRI data of healthy older individuals as acquired in a typical clinical setting.

Materials and Methods

Subjects

Imaging data were obtained from the Nathan Kline Institute (NKI) / Rockland sample (Nooner, et al., 2012), available through the International Neuroimaging Data-Sharing Initiative (INDI, http://fcon_1000.projects.nitrc.org). From this population-based cohort (N=207) we first selected all subjects with an age over 17 years as well as no current or lifetime diagnosis of mental disorders according to the Diagnostic and Statistical Manual of Mental Disorders (DSM-IV-TR; American Psychiatric Association, 2000) (N=105). Two subjects were rejected due to missing information regarding the DSM-IV-TR information and one subject was rejected due to missing structural imaging data. After preprocessing (see below), we excluded the imaging data of subjects with more than 2mm and 2° in maximum head motion (N = 17). In total, eighty-five subjects (age range: 19-85 years, 47 males) were included in the parcellation procedure.

For validation purposes we applied our parcellation results on rs-fMRI data of an independent sample derived from our local cohort of healthy elderly volunteers recruited at the DZNE in Rostock (N = 25, age range: 65-89 years, 13 males). Acquisition parameters and preprocessing procedures for the 3T MRI data of this sample has previously been described in detail (Dyrba, et al., 2015) and followed similar settings as described for the NKI/Rockland sample in the next sections.

Image acquisition

Ten-minute rs-fMRI scans were obtained from all subjects on a single 3T Siemens MRI scanner (Magnetom TrioTim, Siemens Medical Systems, Erlangen, Germany) using an echo planar imaging (EPI) sequence with the following parameters: orientation = transversal, FoV = 216 mm, voxel size = 3.0 mm isotropic, slice thickness = 3.0 mm, repetition time = 2500

For anatomic reference and image preprocessing, high-resolution structural MRI (sMRI) scans were obtained using the same scanner and a magnetization prepared rapid acquisition gradient echo (MPRAGE) sequence with the following parameters: orientation = sagittal, FoV = 256 mm, voxel size = 1.0 mm isotropic, slice thickness = 1.0 mm, repetition time = 2500 ms, echo time = 3.5 ms, flip angle 8°.

Preprocessing

We used the advanced version of the Data Processing Assistant for Resting-State fMRI (DPARSFA; (Chao-Gan and Yu-Feng, 2010)) in conjunction with the statistical parametric mapping software (SPM8, http://www.fil.ion.ucl.ac.uk/spm) and the toolbox for Data Processing and Analysis of Brain Imaging (DPABI, http://rfmri.org/DPABI). We first removed the 10 initial time points of the rs-fMRI time-series and applied slice timing correction on the remaining volumes. The slice-timed rs-fMRI volumes were realigned and motion corrected, and the mean volume was coregistered to the corresponding sMRI. Structural MRIs were segmented into gray matter (GM), white matter (WM) and cerebrospinal fluid (CSF) partitions, and spatially normalized to stereotactic Montreal Neurological Institute (MNI) space using DARTEL (Ashburner, 2007). We regressed out nuisance covariates in the rs-fMRIs with 24 head motion parameters (Friston, et al., 1996), as well as global, WM and CSF signal as nuisance regressors, including a linear detrend. Subsequently, rs-fMRIs were normalized to MNI space using the normalization parameters of the coregistered sMRI scans. Finally, the rs-fMRIs were smoothed with a 6mm full width at half maximum (FWHM) Gaussian kernel, masked for cerebral tissue, and bandpass filtered between 0.01 and 0.08 Hz (Logothetis, et al., 2001; Lu, et al., 2007).

Definition of CBF region of interest and functional connectivity analyses

A comprehensive CBF region-of-interest (ROI) was defined in the MNI space template based on combined information from existing stereotactic atlases of basal forebrain cholinergic nuclei in MNI space (Kilimann, et al., 2014; Teipel, et al., 2005; Zaborszky, et al., 2008). This mask was resampled to a final voxel size of 3mm isotropic to match the voxel size of the rs-fMRI images. For each of the 189 voxels in the CBF-mask, we calculated an FC map by correlating the voxel's signal time course with all other GM voxels of the brain (as defined in the Harvard-Oxford atlas for cortical and subcortical regions (Desikan, et al., 2006)). Voxel-specific FC maps were Fisher z-transformed and then averaged over all subjects.

Experimental Design and Statistical Analysis

Connectivity based parcellation

The CBF ROI was parcellated into functionally homogeneous subdivisions by clustering its voxels based on the similarity of their averaged FC maps on group-level using the k-means clustering algorithm (Eickhoff, et al., 2016; Lloyd, 1982). For this, the data was first organized into an n-by-m matrix representing the FC maps of all CBF voxels, where n represents the voxels in the CBF ROI (189 voxels) and m all other brain GM voxels with their corresponding FC values. Similarity between the voxels' FC maps was estimated using Pearson's correlation coefficient, and one minus the correlation coefficient was used as a distance measure. The k-means clustering algorithm then partitioned the CBF voxels (rows of the n-by-m matrix) by initially assigning all voxels to k different clusters based on centroids positioned by chance, and iteratively reassigning the voxels until the intra-cluster distances across all clusters reached a minimum (maximum 1000 iterations). For each k, the clustering was repeated for 100 random starting positions of the initial centroids, and the best solution was chosen based on the mean silhouette value for all voxels (Kaufman and Rousseeuw, 1990). The silhouette value ranges from -1 to +1 and measures the similarity of a given voxel

In our primary analysis we set $k = 2$, because we hypothesized that the well-described cortical projection differences between anterior-medial (MS, DB) and posterior-lateral (NBM) CBF subdivisions in animal models (Luiten, et al., 1987; Mesulam, et al., 1983a) would be detected as differential rs-fMRI FC profiles in the human CBF. In additional analysis using $k = 3$ and $k = 4$, we further explored the feasibility of using rs-fMRI data for detecting even more fine grained functional distinctions among CBF divisions in the human brain.

Cluster-wise functional connectivity

For each cluster of the final CBF parcellations we determined the specific FC profile leading to the definition of that cluster. Cluster-to-voxel FC maps were calculated for each individual and subjected to second-level one-sample t-tests, using age and gender as covariates, and restricting the search space to the GM mask that was also used for the FC maps driving the CBF parcellation. Due to the uncertain interpretation of negative time course correlations (anticorrelations) that can emerge as an artifact of global signal regression, we only considered positive effects in the FC maps (Murphy and Fox, 2017). Results are reported at a voxel-wise statistical threshold of $p < 0.05$, corrected for multiple testing using the family-wise error rate (FWE).

Given animal-derived evidence for a functional topography of CBF projections that follows the organization of inter-connected cortical systems (Ghashghaei and Barbas, 2001; Zaborszky, et al., 2015), we further analyzed FC profiles of the CBF in relation to functional brain networks using an established parcellation of the human cerebral cortex into 17 intrinsically connected networks (Yeo, et al., 2011). For each subject, the CBF clusters' signal time courses were correlated with the average signal time course of each of the 17 networks. These correlations were Fisher z-transformed, and significance of their deviance

Effects of age on cluster-wise functional connectivity

Effects of age on CBF FC were assessed for the two principal CBF subdivisions revealed by the $k = 2$ clustering parcellation. Analyses employed voxel-wise linear regressions of age on cluster-specific FC maps and were controlled for gender. The search space was restricted to the thresholded positive connectivity profile of each CBF cluster and statistical significance was assessed at $p < 0.05$, corrected for the false discovery rate (FDR).

Replication of cluster-wise functional connectivity profiles in an independent sample

For the two principal CBF subdivisions identified in our primary analysis we calculated cluster-wise FC profiles within the independent replication sample using FC analyses as described above. Topographic correspondence between the cluster-wise FC profiles derived from the two independent samples was quantified using spatial correlation (Pearson's r) of the sample-specific FC signals across all cortical networks (Buckner, et al., 2009; Fjell, et al., 2015; Grothe and Teipel, 2016).

Results

Connectivity based parcellation

K-means clustering for k = 2 parcellated the CBF into an anterior-medial cluster (aCBF) and a posterior-lateral cluster (pCBF; Fig. 1). The aCBF cluster mostly covered the rostral nuclei of the MS/DB but also included anterior-medial parts of the NBM (Fig. 1A), and was characterized by predominant FC with the hippocampus, ventromedial prefrontal cortex and retrosplenial/posterior cingulate cortex (Fig. 1B, Table I). The pCBF cluster covered the remaining anterior-lateral, intermediate and posterior parts of the NBM (Fig. 1A), and markedly differed in its FC profile from the aCBF cluster; there was more pronounced connectivity with the insula, dorsal anterior cingulate cortex (dACC) and thalamus, and an absence of effects in posterior medial cortical areas (Figs. 1B and 5, Table I). The clusters had overlapping FC within regions of the medial prefrontal and (posterior) lateral orbitofrontal cortex, temporal pole, as well as hippocampus and amygdala.

At higher cluster numbers (k = 3 and 4), the aCBF cluster was further partitioned into two and three subclusters, whereas the pCBF cluster remained virtually unchanged (Fig. 2). The first partition (k = 3) separated a region corresponding to anterior-medial parts of the NBM that was characterized by a more selective FC profile with anterior medial temporal and ventromedial prefrontal regions compared to the parent cluster (k3_2; blue cluster in upper part of Fig. 2). The second partition (k = 4) further subdivided the remainder of the aCBF cluster along a horizontal axis anterior to the crossing of the anterior commissure, though the resulting dorsal and ventral subclusters were characterized by very similar FC profiles (k4_1 and k4_2; cyan and orange clusters in bottom part of Fig. 2).

Connectivity with cortical networks

We further characterized the distinct FC profiles of the principal aCBF and pCBF clusters wise profiles, the aCBF cluster showed significant positive FC with limbic networks centered on orbitofrontal ($t(84) = 16.8$, $p < 0.001$) and anterior medial temporal cortices ($t(84) = 8.9$, $p < 0.001$), as well as with midline ($t(84) = 6.2$, $p < 0.001$) and posterior medial temporal subsystems of the default mode network (DMN) ($t(84) = 5.1$, $p < 0.001$). The pCBF cluster also showed positive FC with the anterior medial temporal limbic network ($t(84) = 15.5$, $p < 0.001$), but differed from the aCBF cluster in showing selective FC with the posterior ventral attention network (VAN) ($t(84) = 9.6$, $p < 0.001$), as well as with lateral-temporal parts of the DMN ($t(84) = 6.5$, $p < 0.001$) and the ventrolateral somatomotor network ($t(84) = 6.4$, $p < 0.001$).

Subregion-specific effects of age

Voxel-wise effects of age on FC of the aCBF and pCBF subdivisions are shown in Fig. 4. For the aCBF, higher age was associated with lower FC with the ventromedial prefrontal cortex, hippocampus, and the basal ganglia. For the pCBF, higher age was associated with lower FC with the dACC, anterior insula, lateral orbitofrontal cortex, and basal ganglia.

Replication sample

Seed-based FC analyses in the replication sample produced very similar FC profiles of the aCBF and pCBF subdivisions as initially identified in the NKI/Rockland sample (Fig. 5). When quantified in a spatial correlation analysis across all cortical networks, the respective FC profiles of the aCBF ($r(15) = 0.84$, $p < 0.001$) and pCBF ($r(15) = 0.83$, $p < 0.001$) subdivisions were highly correlated between both samples.

Discussion

CBF subdivisions and their respective functional connectivity profiles

In line with our initial hypothesis, a two-cluster solution parcellated the CBF into distinct anterior-medial and posterior-lateral clusters that were characterized by largely differing FC profiles. Although these clusters were automatically defined based solely on FC characteristics and not constrained by any predefined segments or manual groupings, their boundary shows a striking anatomic resemblance with the distinction between cytoarchitectonically-defined MS/DB (Ch1-3) and NBM (Ch4) subdivisions as revealed by stereotactic mappings (Zaborszky et al., 2008; Kilimann et al., 2014). However, this correspondence between functionally and cytoarchitectonically-defined subdivisions was not complete, given that the aCBF cluster also covered anterior-medial parts of the NBM, whereas the pCBF cluster covered the remaining anterior-lateral, intermediate and posterior parts of the NBM. The aCBF cluster showed FC predominantly with the hippocampus, ventromedial prefrontal cortex and retrosplenial/posterior cingulate cortex, whereas the pCBF cluster showed selective FC with the insula, dACC and thalamus.

According to axonal tracing studies in animal models, posterior CBF neurons (including intermediate and posterior NBM sections) project predominantly to the lateral neo- and mesocortex, particularly the ventrolateral orbital cortex, insula, and temporal pole (Luiten, et al., 1987; Mesulam, et al., 1983a), and these sites are also dominantly represented in our observed pCBF FC profile. In contrast to the pCBF-dACC connectivity observed here, the ACC has been reported to receive cholinergic input primarily from anterior-medial parts of the NBM (Mesulam, et al., 1983a). However, a recent detailed topographic mapping study between CBF neurons and medial prefrontal cortex in mice indicated that this may only be true for the ventral ACC, whereas the dACC was found to be most densely connected with more posterior CBF neurons (Bloem, et al., 2014). Furthermore, the prominent insula-dACC-

FC profile of the NBM reported in a previous study using an a priori seed region based on a cytoarchitectonically-defined stereotactic map (Li, et al., 2014). While axonal tracing studies have documented selective projections from the NBM into the thalamic reticular nucleus (Hallanger, et al., 1987; Levey, et al., 1987), the main cholinergic innervation of the thalamus does not arise from the CBF but from cholinergic nuclei within the brainstem (Ch5/6) (Mesulam, et al., 1983b). Thus, the pCBF/NBM-thalamus connectivity observed in rs-fMRI data may also reflect an indirect functional connection mediated by the common implication of these structures in a larger functional brain network (see further discussion below). While only very limited data on FC characteristics of anterior-medial parts of the CBF is available from one recent rs-fMRI study (Markello, et al., 2018), the observed profile of most pronounced aCBF FC with the hippocampus and interconnected areas of the retrosplenial/posterior cingulate and ventromedial prefrontal cortex is well in line with this recent study and largely agrees with the axonal tracing literature on cortical projection patterns of the anterior CBF nuclei (Bloem, et al., 2014; Gaykema, et al., 1990; Mesulam, et al., 1983a; Parvizi, et al., 2006).

Although the aCBF and pCBF subdivisions are characterized by largely diverging cortical FC profiles, they also show a notable convergence in connectivity within areas of the posterior ventromedial prefrontal cortex, temporal pole, and especially hippocampus and amygdala. Besides receiving the most dense cholinergic innervation among all brain regions (Mesulam, et al., 1986), these key limbic and paralimbic structures are also the only cortical areas that provide neural input into the CBF (Mesulam and Mufson, 1984). A limitation of the FC metric employed in our human in-vivo study is that it cannot distinguish the signaling direction of the functional connection. Future studies may employ effective connectivity paradigms based on experimentally evoked brain activity to further explore the directionality of the identified CBF-cortical connectivity profiles (Friston, et al., 2017).

Relation to cortical functional networks

Visually the aCBF FC profile resembles a previously described medial temporal DMN subsystem/episodic memory network (Andrews-Hanna, et al., 2010; Vincent, et al., 2006), whereas the prominent insula/dACC components of the pCBF FC profile are characteristic of a distinct network that has been variably referred to as VAN, salience, or cingulo-opercular network (Dosenbach, et al., 2007; Seeley, et al., 2007). This network-specific connectivity of aCBF and pCBF subdivisions could also be confirmed by quantitative assessment using standardized templates of well-described cortical brain networks (Yeo, et al., 2011). Interestingly, a specific connectivity of the pCBF with the VAN agrees with findings from a previous molecular imaging study demonstrating a disproportionately high density of cortical nicotinergic receptors in this particular brain network (Picard, et al., 2013).

In general, the finding of network-specific FC profiles of the identified aCBF and pCBF subdivisions coincides with previous evidence from axonal tracing studies in animal models indicating a functionally-based topographical organization of CBF projections (Zaborszky, et al., 2015). Thus, the cortical projection patterns of distinct CBF subdivisions appear to be determined by the functional relatedness and inter-connectivity of the cortical target areas, rather than following strict anatomic gradients of spatial adjacency. It has been hypothesized that this complex corticotopic organization of CBF projections might facilitate coordinate control of spatially separated but functionally linked nodes of large-scale cortical networks (Ballinger, et al., 2016).

The specific FC of the aCBF with the medial temporal DMN/episodic memory network and of the pCBF with the VAN matches the assumed roles of these CBF subdivisions in particular cognitive functions, as revealed by selective lesion studies in animal models. Thus, septohippocampal projections of the anterior CBF have been specifically implicated in memory processes, whereas the neocortical projections of the NBM appear to be more

Future studies combining in-vivo FC measures of the identified CBF subdivisions with detailed psychometric assessments may allow studying in more detail the role of CBF signaling in human cognition, thereby complementing analogous covariance-based studies on the cognitive correlates of structural CBF decline in aging and neurodegenerative disease (Butler, et al., 2012; Grothe, et al., 2016; Ray, et al., 2015).

More fine-grained CBF parcellations

Surprisingly, higher cluster solutions did not result in an increasing parcellation of the pCBF cluster covering different cytoarchitectonic NBM subdivisions, but further fractionated the aCBF cluster. In a first step, this resulted in a separation of a region corresponding to anterior-medial parts of the NBM, which was characterized by a more selective FC profile with anterior medial temporal and ventromedial prefrontal regions compared to the parent cluster. Among all NBM neurons, the anterior-medial populations show the strongest axonal projections to the hippocampus and ventromedial cortex in animal models, and accordingly this subdivision has been described as a transitional zone between the anterior and posterior CBF (Luiten, et al., 1987; Mesulam, et al., 1983a). In a second step, the most anterior medial cluster further split along a horizontal axis at the level of the anterior commissure, which may potentially reflect connectivity differences between the MS/vertical DB and the horizontal DB. However, in contrast to the parcellated subdivisions identified in the previous steps, this distinction was only based on very subtle differences in the respective FC profiles. In this context it has to be noted that the employed clustering approach is explorative in nature and the correct number of meaningful subdivisions is not known a priori. Rather, the approach allows exploring regional differences in FC characteristics across increasing parcellation resolutions. The marginal difference in FC profiles at the highest examined clustering solution indicates that this resolution may represent a limit for resolving meaningful acquisitions. Future studies using ultra-high field fMRI acquisitions may potentially further improve the corticotopic mapping of human CBF connectivity (Maass, et al., 2015).

Rs-fMRI CBF connectivity as an in-vivo marker of alterations in CBF function

We demonstrated the potential of using rs-fMRI to investigate alterations in CBF function by showing a significant age-related decline in subregion-specific CBF FC. This finding may reflect the well-described decrease in cholinergic tone during normal brain aging, which is believed to underlie subtle impairments in cognition and a higher susceptibility to anticholinergic side effects (Risacher, et al., 2016; Schliebs and Arendt, 2011). Most interestingly, despite both CBF subdivisions showing prominent connectivity to the hippocampus, only the hippocampal connectivity of the aCBF subdivision was negatively affected by advancing age. While this finding nicely coincides with the marked age effects on cholinergic septohippocampal projections described in animal models (Ypsilanti, et al., 2008), it has to be noted that our in-vivo connectivity approach cannot distinguish between cholinergic and non-cholinergic neuron populations in the examined CBF-mask. Although definition of this region was based on stereotactic mappings of histologically determined CBF nuclei in the human brain (Kilimann, et al., 2014; Teipel, et al., 2005; Zaborszky, et al., 2008), this brain area also contains non-cholinergic, particularly GABAergic, projection neurons that may show similar age-related changes (Rubio, et al., 2012; Yang, et al., 2017). Irrespective of this limitation, these findings underline the importance of using functionally homogeneous seed regions when studying age or disease-related CBF connectivity alterations with rs-fMRI, similar to what has been reported for FC studies focused on the hippocampus and posterior cingulate cortex (Damoiseaux, et al., 2016; Dillen, et al., 2016).

Conclusion

Our study paves the way for using rs-fMRI-based assessments of subregion-specific CBF function to complement established volumetric approaches in the in-vivo study of CBF involvement in cognitive aging and neurodegenerative disease (Grothe, et al., 2012; Schmitz and Spreng, 2016). As a first step towards such applications we demonstrated that the dissociated FC profiles of the identified CBF subdivisions are reproducible in rs-fMRI acquisitions of elderly participants as typically collected in clinical research settings. We expect rs-fMRI-based assessments of CBF connectivity to be particularly useful for the study of functional CBF alterations in predementia stages of neurodegenerative disease (Brayda-Bruno, et al., 2013; Grothe, et al., 2014; Lim, et al., 2015; Ray, et al., 2017), as well as other neuropsychiatric conditions with cholinergic involvement that are not typically associated with gross neurodegeneration (Grothe, et al., 2017; Perry, et al., 2001; Sarter, et al., 2012).

References

Andrews-Hanna, J.R., Reidler, J.S., Sepulcre, J., Poulin, R., Buckner, R.L. (2010) Functional-anatomic fractionation of the brain's default network. Neuron, 65:550-62.

Ashburner, J. (2007) A fast diffeomorphic image registration algorithm. Neuroimage, 38:95-113.

Ballinger, E.C., Ananth, M., Talmage, D.A., Role, L.W. (2016) Basal Forebrain Cholinergic Circuits and Signaling in Cognition and Cognitive Decline. Neuron, 91:1199-218.

Berger-Sweeney, J., Stearns, N.A., Murg, S.L., Floerke-Nashner, L.R., Lappi, D.A., Baxter, M.G. (2001) Selective immunolesions of cholinergic neurons in mice: effects on neuroanatomy, neurochemistry, and behavior. The Journal of neuroscience : the official journal of the Society for Neuroscience, 21:8164-73.

Bloem, B., Schoppink, L., Rotaru, D.C., Faiz, A., Hendriks, P., Mansvelder, H.D., van de Berg, W.D., Wouterlood, F.G. (2014) Topographic mapping between basal forebrain cholinergic neurons and the medial prefrontal cortex in mice. The Journal of neuroscience : the official journal of the Society for Neuroscience, 34:16234-46.

Brayda-Bruno, L., Mons, N., Yee, B.K., Micheau, J., Abrous, D.N., Nogues, X., Marighetto, A. (2013) Partial loss in septo-hippocampal cholinergic neurons alters memory-dependent measures of brain connectivity without overt memory deficits. Neurobiol Dis, 54:372-81.

Buckner, R.L., Sepulcre, J., Talukdar, T., Krienen, F.M., Liu, H., Hedden, T., Andrews-Hanna, J.R., Sperling, R.A., Johnson, K.A. (2009) Cortical hubs revealed by intrinsic functional connectivity: mapping, assessment of stability, and relation to Alzheimer's disease. The Journal of neuroscience : the official journal of the Society for Neuroscience, 29:1860-73.

Butler, T., Blackmon, K., Zaborszky, L., Wang, X., DuBois, J., Carlson, C., Barr, W.B., the human septal forebrain region is a predictor of source memory accuracy. J Int Neuropsychol Soc, 18:157-61.

Chao-Gan, Y., Yu-Feng, Z. (2010) DPARSF: A MATLAB Toolbox for "Pipeline" Data Analysis of Resting-State fMRI. Frontiers in systems neuroscience, 4:13.

Damoiseaux, J.S., Viviano, R.P., Yuan, P., Raz, N. (2016) Differential effect of age on posterior and anterior hippocampal functional connectivity. Neuroimage, 133:468-76.

Desikan, R.S., Segonne, F., Fischl, B., Quinn, B.T., Dickerson, B.C., Blacker, D., Buckner, R.L., Dale, A.M., Maguire, R.P., Hyman, B.T., Albert, M.S., Killiany, R.J. (2006) An automated labeling system for subdividing the human cerebral cortex on MRI scans into gyral based regions of interest. Neuroimage, 31:968-80.

Dillen, K.N.H., Jacobs, H.I.L., Kukolja, J., von Reutern, B., Richter, N., Onur, O.A., Dronse, J., Langen, K.J., Fink, G.R. (2016) Aberrant functional connectivity differentiates retrosplenial cortex from posterior cingulate cortex in prodromal Alzheimer's disease. Neurobiol Aging, 44:114-126.

Dosenbach, N.U., Fair, D.A., Miezin, F.M., Cohen, A.L., Wenger, K.K., Dosenbach, R.A., Fox, M.D., Snyder, A.Z., Vincent, J.L., Raichle, M.E., Schlaggar, B.L., Petersen, S.E. (2007) Distinct brain networks for adaptive and stable task control in humans. Proc Natl Acad Sci U S A, 104:11073-8.

Dyrba, M., Grothe, M., Kirste, T., Teipel, S.J. (2015) Multimodal analysis of functional and structural disconnection in Alzheimer's disease using multiple kernel SVM. Human brain mapping, 36:2118-31.

Eickhoff, S.B., Laird, A.R., Fox, P.T., Bzdok, D., Hensel, L. (2016) Functional Segregation of the Human Dorsomedial Prefrontal Cortex. Cerebral cortex, 26:304-21.

Eickhoff, S.B., Thirion, B., Varoquaux, G., Bzdok, D. (2015) Connectivity-based parcellation: Critique and implications. Human brain mapping, 36:4771-92.

Englot, D.J., D'Haese, P.F., Konrad, P.E., Jacobs, M.L., Gore, J.C., Abou-Khalil, B.W., Morgan, V.L. (2017) Functional connectivity disturbances of the ascending reticular activating system in temporal lobe epilepsy. J Neurol Neurosurg Psychiatry.

Fjell, A.M., Amlien, I.K., Sneve, M.H., Grydeland, H., Tamnes, C.K., Chaplin, T.A., Rosa, M.G., Walhovd, K.B. (2015) The Roots of Alzheimer's Disease: Are High-Expanding Cortical Areas Preferentially Targeted?dagger. Cereb Cortex, 25:2556-65.

Friston, K.J., Preller, K.H., Mathys, C., Cagnan, H., Heinzle, J., Razi, A., Zeidman, P. (2017) Dynamic causal modelling revisited. NeuroImage.

Friston, K.J., Williams, S., Howard, R., Frackowiak, R.S., Turner, R. (1996) Movement-related effects in fMRI time-series. Magnetic resonance in medicine, 35:346-55.

Gaykema, R.P., Luiten, P.G., Nyakas, C., Traber, J. (1990) Cortical projection patterns of the medial septum-diagonal band complex. The Journal of comparative neurology, 293:103-24.

Ghashghaei, H.T., Barbas, H. (2001) Neural interaction between the basal forebrain and functionally distinct prefrontal cortices in the rhesus monkey. Neuroscience, 103:593-614.

Grothe, M., Heinsen, H., Teipel, S.J. (2012) Atrophy of the cholinergic Basal forebrain over the adult age range and in early stages of Alzheimer's disease. Biological psychiatry, 71:805-13.

Grothe, M.J., Ewers, M., Krause, B., Heinsen, H., Teipel, S.J. (2014) Basal forebrain atrophy and cortical amyloid deposition in nondemented elderly subjects. Alzheimer's & dementia : the journal of the Alzheimer's Association, 10:S344-53.

Grothe, M.J., Heinsen, H., Amaro, E., Jr., Grinberg, L.T., Teipel, S.J. (2016) Cognitive Correlates of Basal Forebrain Atrophy and Associated Cortical Hypometabolism in Mild Cognitive Impairment. Cerebral cortex (New York, N.Y. : 1991), 26:2411-2426.

Grothe, M.J., Scheef, L., Bauml, J., Meng, C., Daamen, M., Baumann, N., Zimmer, C., Teipel, S., Bartmann, P., Boecker, H., Wolke, D., Wohlschlager, A., Sorg, C. (2017) Reduced Cholinergic Basal Forebrain Integrity Links Neonatal Complications and Adult Cognitive Deficits After Premature Birth. Biol Psychiatry, 82:119-126.

Grothe, M.J., Teipel, S.J. (2016) Spatial patterns of atrophy, hypometabolism, and amyloid deposition in Alzheimer's disease correspond to dissociable functional brain networks. Human brain mapping, 37:35-53.

Hallanger, A.E., Levey, A.I., Lee, H.J., Rye, D.B., Wainer, B.H. (1987) The origins of cholinergic and other subcortical afferents to the thalamus in the rat. The Journal of comparative neurology, 262:105-24.

Hansson, O., Grothe, M.J., Strandberg, T.O., Ohlsson, T., Hagerstrom, D., Jogi, J., Smith, R., Scholl, M. (2017) Tau Pathology Distribution in Alzheimer's disease Corresponds Differentially to Cognition-Relevant Functional Brain Networks. Frontiers in neuroscience, 11:167.

Hasselmo, M.E., Sarter, M. (2011) Modes and models of forebrain cholinergic neuromodulation of cognition. Neuropsychopharmacology, 36:52-73.

Hedreen, J.C., Struble, R.G., Whitehouse, P.J., Price, D.L. (1984) Topography of the magnocellular basal forebrain system in human brain. J Neuropathol Exp Neurol, 43:1-21.

Kahnt, T., Chang, L.J., Park, S.Q., Heinzle, J., Haynes, J.D. (2012) Connectivity-based parcellation of the human orbitofrontal cortex. The Journal of neuroscience : the official journal of the Society for Neuroscience, 32:6240-50.

Kaufman, L., Rousseeuw, P.J. (1990) Finding groups in data: an introduction to cluster analysis.

Kilimann, I., Grothe, M., Heinsen, H., Alho, E.J., Grinberg, L., Amaro, E., Jr., Dos Santos, M., Hampel, H., Kloppel, S., Teipel, S.J. (2014) Subregional basal forebrain atrophy in Alzheimer's disease: a multicenter study. Journal of Alzheimer's disease : JAD, 40:687-700.

Kitt, C.A., Mitchell, S.J., DeLong, M.R., Wainer, B.H., Price, D.L. (1987) Fiber pathways of basal forebrain cholinergic neurons in monkeys. Brain research, 406:192-206.

Levey, A.I., Hallanger, A.E., Wainer, B.H. (1987) Cholinergic nucleus basalis neurons may influence the cortex via the thalamus. Neuroscience letters, 74:7-13.

Li, C.S., Ide, J.S., Zhang, S., Hu, S., Chao, H.H., Zaborszky, L. (2014) Resting state functional connectivity of the basal nucleus of Meynert in humans: in comparison to the ventral striatum and the effects of age. NeuroImage, 97:321-32.

Libby, L.A., Ekstrom, A.D., Ragland, J.D., Ranganath, C. (2012) Differential connectivity of perirhinal and parahippocampal cortices within human hippocampal subregions revealed by high-resolution functional imaging. The Journal of neuroscience : the official journal of the Society for Neuroscience, 32:6550-60.

Lim, Y.Y., Maruff, P., Schindler, R., Ott, B.R., Salloway, S., Yoo, D.C., Noto, R.B., Santos, C.Y., Snyder, P.J. (2015) Disruption of cholinergic neurotransmission exacerbates Abeta-related cognitive impairment in preclinical Alzheimer's disease. Neurobiol Aging, 36:2709-15.

Lloyd, S.P. (1982) Least-Squares Quantization in Pcm. Ieee T Inform Theory, 28:129-137.

Logothetis, N.K., Pauls, J., Augath, M., Trinath, T., Oeltermann, A. (2001) Neurophysiological investigation of the basis of the fMRI signal. Nature, 412:150-7.

Lu, H., Zuo, Y., Gu, H., Waltz, J.A., Zhan, W., Scholl, C.A., Rea, W., Yang, Y., Stein, E.A. (2007) Synchronized delta oscillations correlate with the resting-state functional MRI signal. Proceedings of the National Academy of Sciences of the United States of America, 104:18265-9.

Luiten, P.G., Gaykema, R.P., Traber, J., Spencer, D.G., Jr. (1987) Cortical projection patterns of magnocellular basal nucleus subdivisions as revealed by anterogradely transported Phaseolus vulgaris leucoagglutinin. Brain research, 413:229-50.

Maass, A., Berron, D., Libby, L.A., Ranganath, C., Duzel, E. (2015) Functional subregions of the human entorhinal cortex. Elife, 4.

Markello, R.D., Spreng, R.N., Luh, W.M., Anderson, A.K., De Rosa, E. (2018) Segregation of the human basal forebrain using resting state functional MRI. NeuroImage, 173:287-297.

Mesulam, M.M., Geula, C. (1988) Nucleus basalis (Ch4) and cortical cholinergic innervation in the human brain: observations based on the distribution of acetylcholinesterase and choline acetyltransferase. The Journal of comparative neurology, 275:216-40.

Mesulam, M.M., Hersh, L.B., Mash, D.C., Geula, C. (1992) Differential cholinergic innervation within functional subdivisions of the human cerebral cortex: a choline acetyltransferase study. The Journal of comparative neurology, 318:316-28.

Mesulam, M.M., Mufson, E.J. (1984) Neural inputs into the nucleus basalis of the substantia innominata (Ch4) in the rhesus monkey. Brain, 107 (Pt 1):253-74.

Mesulam, M.M., Mufson, E.J., Levey, A.I., Wainer, B.H. (1983a) Cholinergic innervation of cortex by the basal forebrain: cytochemistry and cortical connections of the septal area, diagonal band nuclei, nucleus basalis (substantia innominata), and hypothalamus in the rhesus monkey. The Journal of comparative neurology, 214:170-97.

Mesulam, M.M., Mufson, E.J., Wainer, B.H., Levey, A.I. (1983b) Central cholinergic pathways in the rat: an overview based on an alternative nomenclature (Ch1-Ch6). Neuroscience, 10:1185-201.

Mesulam, M.M., Volicer, L., Marquis, J.K., Mufson, E.J., Green, R.C. (1986) Systematic regional differences in the cholinergic innervation of the primate cerebral cortex:

distribution of enzyme activities and some behavioral implications. Ann Neurol, 19:144-51.

Mishra, A., Rogers, B.P., Chen, L.M., Gore, J.C. (2014) Functional connectivity-based parcellation of amygdala using self-organized mapping: a data driven approach. Human brain mapping, 35:1247-60.

Murphy, K., Fox, M.D. (2017) Towards a consensus regarding global signal regression for resting state functional connectivity MRI. NeuroImage, 154:169-173.

Nooner, K.B., Colcombe, S.J., Tobe, R.H., Mennes, M., Benedict, M.M., Moreno, A.L., Panek, L.J., Brown, S., Zavitz, S.T., Li, Q., Sikka, S., Gutman, D., Bangaru, S., Schlachter, R.T., Kamiel, S.M., Anwar, A.R., Hinz, C.M., Kaplan, M.S., Rachlin, A.B., Adelsberg, S., Cheung, B., Khanuja, R., Yan, C., Craddock, C.C., Calhoun, V., Courtney, W., King, M., Wood, D., Cox, C.L., Kelly, A.M., Di Martino, A., Petkova, E., Reiss, P.T., Duan, N., Thomsen, D., Biswal, B., Coffey, B., Hoptman, M.J., Javitt, D.C., Pomara, N., Sidtis, J.J., Koplewicz, H.S., Castellanos, F.X., Leventhal, B.L., Milham, M.P. (2012) The NKI-Rockland Sample: A Model for Accelerating the Pace of Discovery Science in Psychiatry. Frontiers in neuroscience, 6:152.

Parvizi, J., Van Hoesen, G.W., Buckwalter, J., Damasio, A. (2006) Neural connections of the posteromedial cortex in the macaque. Proc Natl Acad Sci U S A, 103:1563-8.

Pascual, B., Masdeu, J.C., Hollenbeck, M., Makris, N., Insausti, R., Ding, S.L., Dickerson, B.C. (2015) Large-scale brain networks of the human left temporal pole: a functional connectivity MRI study. Cerebral cortex, 25:680-702.

Perry, E.K., Lee, M.L., Martin-Ruiz, C.M., Court, J.A., Volsen, S.G., Merrit, J., Folly, E., Iversen, P.E., Bauman, M.L., Perry, R.H., Wenk, G.L. (2001) Cholinergic activity in autism: abnormalities in the cerebral cortex and basal forebrain. Am J Psychiatry, 158:1058-66.

Picard, F., Sadaghiani, S., Leroy, C., Courvoisier, D.S., Maroy, R., Bottlaender, M. (2013) High density of nicotinic receptors in the cingulo-insular network. Neuroimage, 79:42-51.

Ray, N.J., Bradburn, S., Murgatroyd, C., Toseeb, U., Mir, P., Kountouriotis, G.K., Teipel, S.J., Grothe, M.J. (2017) In vivo cholinergic basal forebrain atrophy predicts cognitive decline in de novo Parkinson's disease. Brain.

Ray, N.J., Metzler-Baddeley, C., Khondoker, M.R., Grothe, M.J., Teipel, S., Wright, P., Heinsen, H., Jones, D.K., Aggleton, J.P., O'Sullivan, M.J. (2015) Cholinergic basal forebrain structure influences the reconfiguration of white matter connections to support residual memory in mild cognitive impairment. J Neurosci, 35:739-47.

Risacher, S.L., McDonald, B.C., Tallman, E.F., West, J.D., Farlow, M.R., Unverzagt, F.W., Gao, S., Boustani, M., Crane, P.K., Petersen, R.C., Jack, C.R., Jr., Jagust, W.J., Aisen, P.S., Weiner, M.W., Saykin, A.J. (2016) Association Between Anticholinergic Medication Use and Cognition, Brain Metabolism, and Brain Atrophy in Cognitively Normal Older Adults. JAMA Neurol, 73:721-32.

Rogers, J.D., Brogan, D., Mirra, S.S. (1985) The nucleus basalis of Meynert in neurological disease: a quantitative morphological study. Ann Neurol, 17:163-70.

Roy, A.K., Shehzad, Z., Margulies, D.S., Kelly, A.M., Uddin, L.Q., Gotimer, K., Biswal, B.B., Castellanos, F.X., Milham, M.P. (2009) Functional connectivity of the human amygdala using resting state fMRI. Neuroimage, 45:614-26.

Rubio, S.E., Vega-Flores, G., Martinez, A., Bosch, C., Perez-Mediavilla, A., del Rio, J., Gruart, A., Delgado-Garcia, J.M., Soriano, E., Pascual, M. (2012) Accelerated aging of the GABAergic septohippocampal pathway and decreased hippocampal rhythms in a mouse model of Alzheimer's disease. FASEB J, 26:4458-67.

Sarter, M., Lustig, C., Taylor, S.F. (2012) Cholinergic contributions to the cognitive symptoms of schizophrenia and the viability of cholinergic treatments. Neuropharmacology, 62:1544-53.

Schliebs, R., Arendt, T. (2011) The cholinergic system in aging and neuronal degeneration. Behav Brain Res, 221:555-63.

Schmitz, T.W., Spreng, R. (2016) Basal forebrain degeneration precedes and predicts the cortical spread of Alzheimer's pathology. Nat Commun, 7:13249.

Seeley, W.W., Menon, V., Schatzberg, A.F., Keller, J., Glover, G.H., Kenna, H., Reiss, A.L., Greicius, M.D. (2007) Dissociable intrinsic connectivity networks for salience processing and executive control. The Journal of neuroscience : the official journal of the Society for Neuroscience, 27:2349-56.

Selden, N.R., Gitelman, D.R., Salamon-Murayama, N., Parrish, T.B., Mesulam, M.M. (1998) Trajectories of cholinergic pathways within the cerebral hemispheres of the human brain. Brain : a journal of neurology, 121 (Pt 12):2249-57.

Teipel, S.J., Flatz, W.H., Heinsen, H., Bokde, A.L., Schoenberg, S.O., Stockel, S., Dietrich, O., Reiser, M.F., Moller, H.J., Hampel, H. (2005) Measurement of basal forebrain atrophy in Alzheimer's disease using MRI. Brain : a journal of neurology, 128:2626-44.

Vincent, J.L., Snyder, A.Z., Fox, M.D., Shannon, B.J., Andrews, J.R., Raichle, M.E., Buckner, R.L. (2006) Coherent spontaneous activity identifies a hippocampal-parietal memory network. Journal of neurophysiology, 96:3517-31.

Voytko, M.L., Olton, D.S., Richardson, R.T., Gorman, L.K., Tobin, J.R., Price, D.L. (1994) Basal forebrain lesions in monkeys disrupt attention but not learning and memory. The Journal of neuroscience : the official journal of the Society for Neuroscience, 14:167-86.

Whitehouse, P.J., Hedreen, J.C., White, C.L., 3rd, Price, D.L. (1983) Basal forebrain neurons in the dementia of Parkinson disease. Ann Neurol, 13:243-8.

Whitehouse, P.J., Price, D.L., Struble, R.G., Clark, A.W., Coyle, J.T., Delon, M.R. (1982) Alzheimer's disease and senile dementia: loss of neurons in the basal forebrain. Science, 215:1237-9.

Yang, C., Thankachan, S., McCarley, R.W., Brown, R.E. (2017) The menagerie of the basal forebrain: how many (neural) species are there, what do they look like, how do they behave and who talks to whom? Curr Opin Neurobiol, 44:159-166.

Yeo, B.T., Krienen, F.M., Sepulcre, J., Sabuncu, M.R., Lashkari, D., Hollinshead, M., Roffman, J.L., Smoller, J.W., Zollei, L., Polimeni, J.R., Fischl, B., Liu, H., Buckner, R.L. (2011) The organization of the human cerebral cortex estimated by intrinsic functional connectivity. Journal of neurophysiology, 106:1125-65.

Ypsilanti, A.R., Girao da Cruz, M.T., Burgess, A., Aubert, I. (2008) The length of hippocampal cholinergic fibers is reduced in the aging brain. Neurobiol Aging, 29:1666-79.

Zaborszky, L., Csordas, A., Mosca, K., Kim, J., Gielow, M.R., Vadasz, C., Nadasdy, Z. (2015) Neurons in the basal forebrain project to the cortex in a complex topographic organization that reflects corticocortical connectivity patterns: an experimental study based on retrograde tracing and 3D reconstruction. Cerebral cortex, 25:118-37.

Zaborszky, L., Hoemke, L., Mohlberg, H., Schleicher, A., Amunts, K., Zilles, K. (2008) Stereotaxic probabilistic maps of the magnocellular cell groups in human basal forebrain. NeuroImage, 42:1127-41.

Zhang, D., Snyder, A.Z., Shimony, J.S., Fox, M.D., Raichle, M.E. (2010) Noninvasive functional and structural connectivity mapping of the human thalamocortical system. Cerebral cortex, 20:1187-94.

Zhang, S., Hu, S., Chao, H.H., Li, C.S. (2016) Resting-State Functional Connectivity of the Locus Coeruleus in Humans: In Comparison with the Ventral Tegmental Area/Substantia Nigra Pars Compacta and the Effects of Age. Cereb Cortex, 26:3413-27.

Zhuo, J., Fan, L., Liu, Y., Zhang, Y., Yu, C., Jiang, T. (2016) Connectivity Profiles Reveal a Transition Subarea in the Parahippocampal Region That Integrates the Anterior Temporal-Posterior Medial Systems. The Journal of neuroscience : the official journal of the Society for Neuroscience, 36:2782-95.

Figures

Figure 1. Functional connectivity-based CBF parcellation for a two cluster solution.

A. Coronal slices from anterior to posterior showing the anterior-medial (aCBF, green) and posterior-lateral CBF clusters (pCBF, red) identified by k-means clustering ($k = 2$) of voxel-wise functional connectivity profiles. Slice positions are indicated by MNI y-coordinates. B. Corresponding functional connectivity profiles of aCBF and pCBF seeds ($p_{(FWE)} < 0.05$) are illustrated on lateral, medial, and ventral brain surfaces, as well as on representative coronal sections at MNI coordinates $y = -15$, $y = 9$, and $y = 30$.

Figure 2. Functional connectivity-based CBF parcellation at higher cluster solutions.

Figure shows CBF parcellations and corresponding functional connectivity profiles ($p_{(FWE)} < 0.05$) when using higher cluster solutions (k = 3, top row, and k = 4, bottom row) for the k-means clustering algorithm. Analogously to Fig. 1, CBF parcellations are depicted on coronal slices from anterior to posterior spanning MNI coordinates from y = 8 to y = -5. Corresponding functional connectivity profiles are illustrated on lateral, medial, and ventral brain surfaces, as well as on representative coronal sections at MNI coordinates y = -15, y = 9, and y = 30. Violet: k3_1, blue: k3_2 and k4_3, red: k3_3 and k4_4, cyan: k4_1, orange: k4_2.

Figure 3. Functional connectivity of CBF subdivisions with specific cortical networks.

Lines indicate significant positive functional connectivity of the identified anterior-medial (aCBF, green) and posterior-lateral (pCBF, red) CBF subdivisions with specific cortical connectivity networks as defined by standardized network templates (Yeo, et al., 2011). Line thickness indicates effect size.

Figure 4. Effects of age on subregion-specific CBF functional connectivity.

Significant negative effects of age on functional connectivity of the anterior-medial (aCBF, green) and posterior-lateral (pCBF, red) CBF subdivisions are displayed on representative sagittal, coronal and transversal sections of the standard space template ($p_{(FDR)} < 0.05$).

Figure 5. Reproducibility of subregion-specific CBF functional connectivity profiles.

Top and middle panels show unthresholded functional connectivity (FC) maps of the anterior-medial (left side, aCBF) and posterior-lateral (right side, pCBF) CBF clusters derived from the cluster-defining NKI/Rockland sample (top) and the local replication sample of healthy older individuals (middle). FC maps are displayed on representative sagittal, coronal and transversal sections of the standard space template. Confirming the qualitatively visible correspondence between the FC maps, diagrams plotting the respective functional connectivity profiles (expressed as effect size) across 17 cortical networks (Yeo, et al., 2011) show that these are highly correlated between the independent samples (see text for spatial correlation statistics).

Tables

Table I. Locations of local functional connectivity maxima for the anterior and posterior cholinergic basal forebrain (CBF) according to Automated Anatomical Labeling atlas (AAL, http://www.gin.cnrs.fr/en/tools/aal-aal2/). FWE-corrected on voxel-level ($p < 0.05$), minimum cluster-size 20 voxel.

	Cluster-size				MNI coordinate		
Number	[Voxels]	Region	Side	T	x	y	z
		Anterior CBF					
1	3016	Cadaute nucleus	L	33.42	-6	6	-6
		Caudate nucleus	R	29.51	6	12	-6
		Olfactory gyrus	L	17.37	-12	12	-15
2	93	Middle temporal gyrus	R	8.30	57	-6	-18
3	100	Middle temporal gyrus	L	7.95	-57	-3	-21
		Middle temporal gyrus	L	7.68	-51	-12	-18
		Middle temporal gyrus	L	6.04	-63	-15	-18
4	166	Lingual gyrus	L	7.71	-9	-99	-18
		Superior occipital gyrus	R	7.61	18	-105	6
		Inferior occipital gyrus	L	7.05	-21	-99	-12
5	32	Angular gyrus	L	7.22	-48	-75	39
		Angular gyrus	L	6.45	-42	-75	45
		Angular gyrus	L	6.10	-51	-75	30

Table II. Functional connectivity of aCBF and pCBF subdivisions with cortical connectivity networks.

	aCBF			pCBF		
Network	Mean	T	Sig. (2-tailed)	Mean	T	Sig. (2-tailed)
1	0.005	0.198	n.s	-0.101	-5.135	< 0.001
2	-0.057	-2.618	n.s	-0.097	-4.945	< 0.001
3	0.035	1.659	n.s	-0.044	-1.456	n.s
4‡	0.029	1.588	n.s	0.179	6.398	< 0.001
5	-0.128	-6.222	< 0.001	-0.192	-11.910	< 0.001
6	-0.125	-5.935	< 0.001	-0.121	-5.141	< 0.001
7‡	-0.078	-4.433	< 0.001	0.214	9.610	< 0.001
8	-0.175	-8.669	< 0.001	0.042	1.986	n.s
9 †,‡	0.211	8.895	< 0.001	0.313	15.454	< 0.001
10†	0.456	16.763	< 0.001	0.029	1.390	n.s
11	-0.059	-3.089	0.003	-0.179	-9.090	< 0.001
12	-0.217	-12.630	< 0.001	-0.137	-7.675	< 0.001
13	-0.146	-7.494	< 0.001	-0.203	-9.624	< 0.001
14‡	-0.032	-1.963	n.s	0.140	6.464	< 0.001
15†	0.104	5.050	< 0.001	-0.010	-0.567	n.s
16†	0.144	6.233	< 0.001	-0.022	-1.064	n.s
17	0.021	1.012	n.s	0.018	1.017	n.s

Network numbers correspond to their initial description in (Yeo, et al., 2011). According to (Hansson,

† significant positive functional connectivity with aCBF

‡ significant positive functional connectivity with pCBF

n.s. not significant (FDR-corrected alpha = 0.003)

Tables

Table I. Locations of local functional connectivity maxima for the anterior and posterior cholinergic basal forebrain (CBF) according to Automated Anatomical Labeling atlas (AAL, http://www.gin.cnrs.fr/en/tools/aal-aal2/). FWE-corrected on voxel-level ($p < 0.05$), minimum cluster-size 20 voxel.

Number	Cluster-size [Voxels]	Region	Side	T	MNI coordinate x	y	z
		Anterior CBF					
1	3016	Cadaute nucleus	L	33.42	-6	6	-6
		Caudate nucleus	R	29.51	6	12	-6
		Olfactory gyrus	L	17.37	-12	12	-15
2	93	Middle temporal gyrus	R	8.30	57	-6	-18
3	100	Middle temporal gyrus	L	7.95	-57	-3	-21
		Middle temporal gyrus	L	7.68	-51	-12	-18
		Middle temporal gyrus	L	6.04	-63	-15	-18
4	166	Lingual gyrus	L	7.71	-9	-99	-18
		Superior occipital gyrus	R	7.61	18	-105	6
		Inferior occipital gyrus	L	7.05	-21	-99	-12
5	32	Angular gyrus	L	7.22	-48	-75	39
		Angular gyrus	L	6.45	-42	-75	45
		Angular gyrus	L	6.10	-51	-75	30

Table II. Functional connectivity of aCBF and pCBF subdivisions with cortical connectivity networks.

	aCBF			pCBF		
Network	Mean	T	Sig. (2-tailed)	Mean	T	Sig. (2-tailed)
1	0.005	0.198	n.s	-0.101	-5.135	< 0.001
2	-0.057	-2.618	n.s	-0.097	-4.945	< 0.001
3	0.035	1.659	n.s	-0.044	-1.456	n.s
4‡	0.029	1.588	n.s	0.179	6.398	< 0.001
5	-0.128	-6.222	< 0.001	-0.192	-11.910	< 0.001
6	-0.125	-5.935	< 0.001	-0.121	-5.141	< 0.001
7‡	-0.078	-4.433	< 0.001	0.214	9.610	< 0.001
8	-0.175	-8.669	< 0.001	0.042	1.986	n.s
9 †,‡	0.211	8.895	< 0.001	0.313	15.454	< 0.001
10†	0.456	16.763	< 0.001	0.029	1.390	n.s
11	-0.059	-3.089	0.003	-0.179	-9.090	< 0.001
12	-0.217	-12.630	< 0.001	-0.137	-7.675	< 0.001
13	-0.146	-7.494	< 0.001	-0.203	-9.624	< 0.001
14‡	-0.032	-1.963	n.s	0.140	6.464	< 0.001
15†	0.104	5.050	< 0.001	-0.010	-0.567	n.s
16†	0.144	6.233	< 0.001	-0.022	-1.064	n.s
17	0.021	1.012	n.s	0.018	1.017	n.s

Network numbers correspond to their initial description in (Yeo, et al., 2011). According to (Hansson,

[†] significant positive functional connectivity with aCBF

[‡] significant positive functional connectivity with pCBF

n.s. not significant (FDR-corrected alpha = 0.003)

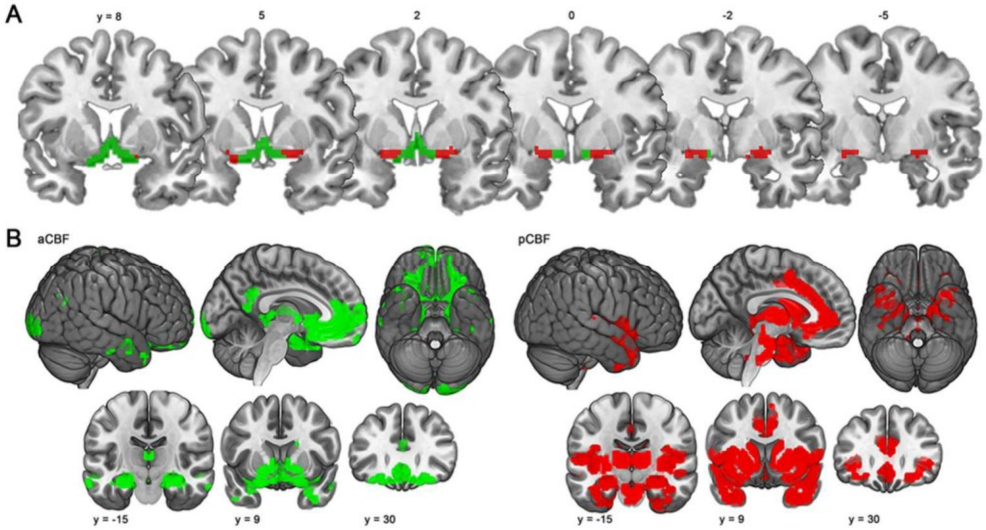

Figure 1. Functional connectivity-based CBF parcellation for a two cluster solution.‼ + A. Coronal slices from anterior to posterior showing the anterior-medial (aCBF, green) and posterior-lateral CBF clusters (pCBF, red) identified by k-means clustering (k = 2) of voxel-wise functional connectivity profiles. Slice positions are indicated by MNI y-coordinates. B. Corresponding functional connectivity profiles of aCBF and pCBF seeds (p(FWE) < 0.05) are illustrated on lateral, medial, and ventral brain surfaces, as well as on representative coronal sections at MNI coordinates y = -15, y = 9, and y = 30.

91x50mm (300 x 300 DPI)

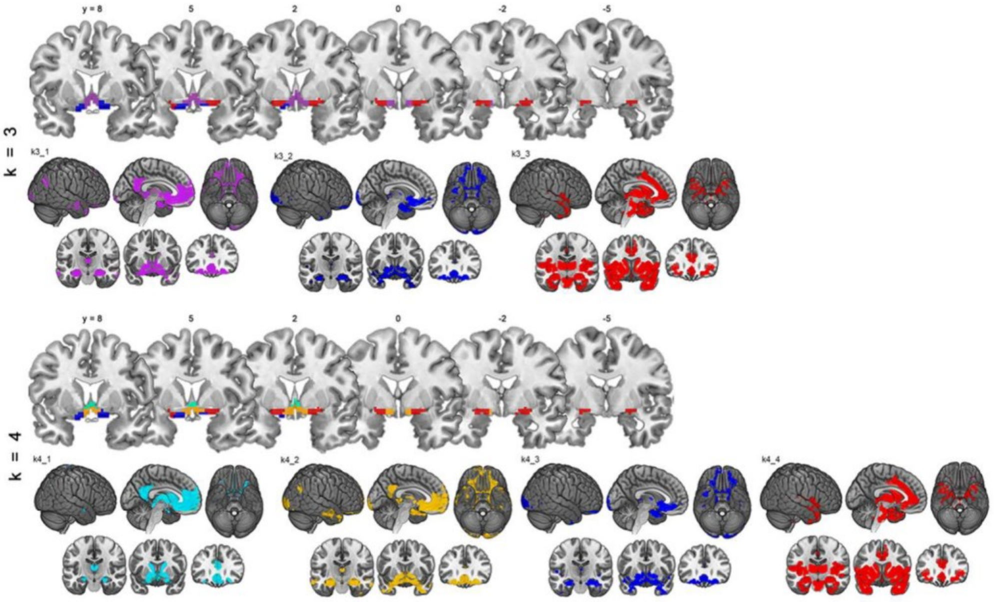

Figure 2. Functional connectivity-based CBF parcellation at higher cluster solutions.
Figure shows CBF parcellations and corresponding functional connectivity profiles (p(FWE) < 0.05) when using higher cluster solutions (k = 3, top row, and k = 4, bottom row) for the k-means clustering algorithm. Analogously to Fig. 1, CBF parcellations are depicted on coronal slices from anterior to posterior spanning MNI coordinates from y = 8 to y = -5. Corresponding functional connectivity profiles are illustrated on lateral, medial, and ventral brain surfaces, as well as on representative coronal sections at MNI coordinates y = -15, y = 9, and y = 30. Violet: k3_1, blue: k3_2 and k4_3, red: k3_3 and k4_4, cyan: k4_1, orange: k4_2.

101x62mm (300 x 300 DPI)

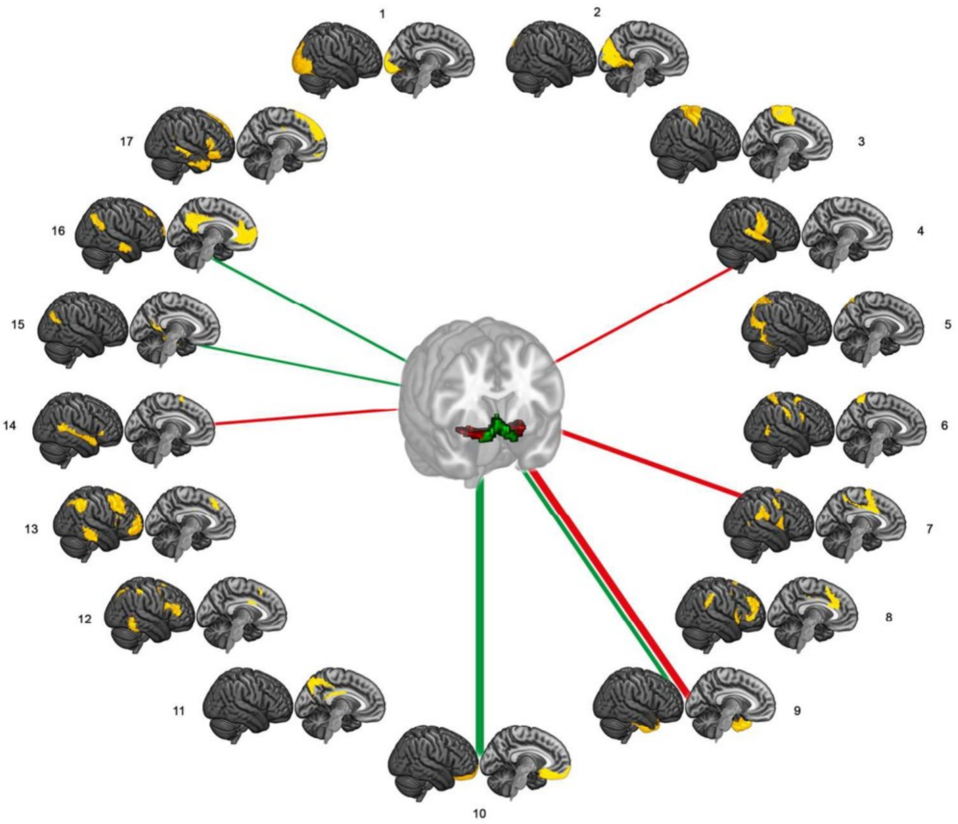

Figure 3. Functional connectivity of CBF subdivisions with specific cortical networks.
Lines indicate significant positive functional connectivity of the identified anterior-medial (aCBF, green) and posterior-lateral (pCBF, red) CBF subdivisions with specific cortical connectivity networks as defined by standardized network templates (Yeo, et al., 2011). Line thickness indicates effect size.

139x117mm (300 x 300 DPI)

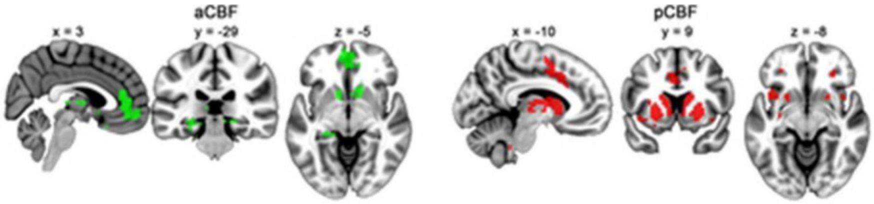

Figure 4. Effects of age on subregion-specific CBF functional connectivity.
Significant negative effects of age on functional connectivity of the anterior-medial (aCBF, green) and posterior-lateral (pCBF, red) CBF subdivisions are displayed on representative sagittal, coronal and transversal sections of the standard space template (p(FDR) < 0.05).

37x8mm (300 x 300 DPI)

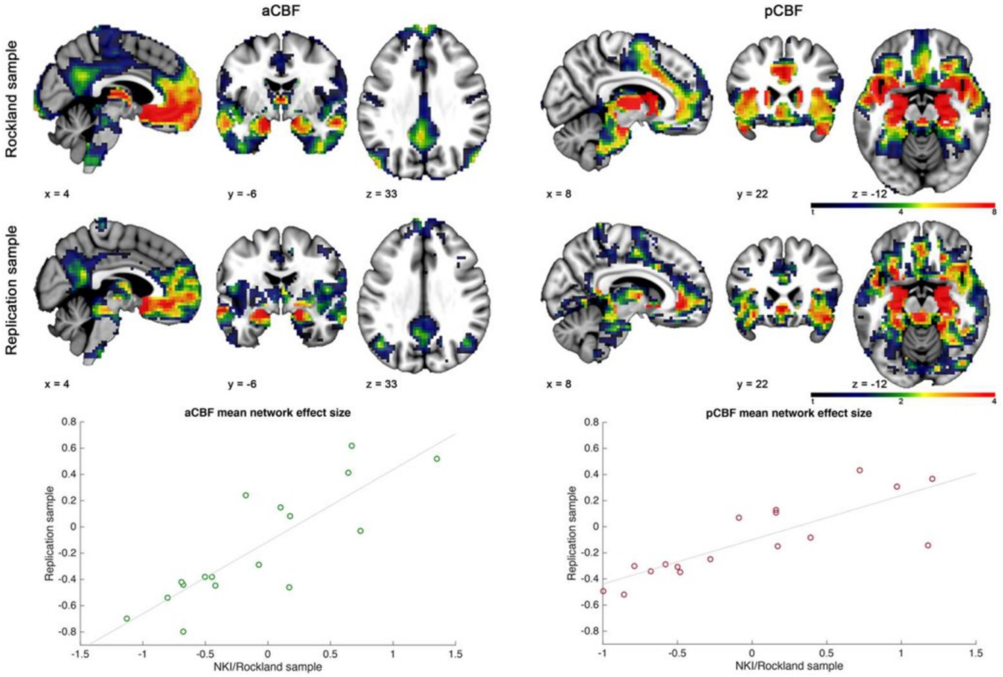

Figure 5. Reproducibility of subregion-specific CBF functional connectivity profiles.
Top and middle panels show unthresholded functional connectivity (FC) maps of the anterior-medial (left side, aCBF) and posterior-lateral (right side, pCBF) CBF clusters derived from the cluster-defining NKI/Rockland sample (top) and the local replication sample of healthy older individuals (middle). FC maps are displayed on representative sagittal, coronal and transversal sections of the standard space template. Confirming the qualitatively visible correspondence between the FC maps, diagrams plotting the respective functional connectivity profiles (expressed as effect size) across 17 cortical networks (Yeo, et al., 2011) show that these are highly correlated between the independent samples (see text for spatial correlation statistics).

111x75mm (300 x 300 DPI)